

Analysis of the dynamic confining effect of CRAC short column under monotonic loadings

Changqing Wang^{*1,2,3,4} and Jianzhuang Xiao^{3a}

¹Jiangsu Key Laboratory of Environmental Impact and Structural Safety in Engineering, China University of Mining & Technology (CUMT), Xuzhou, Jiangsu 221116, China

²Department of Civil Engineering, Shanghai University, Shanghai 200444, China

³Department of Building Engineering, College of Civil Engineering, Tongji University, Shanghai 200092, China

⁴Jiangsu Collaborative Innovation Center for Building Energy Saving and Construction Technology, Xuzhou, Jiangsu 221116, China

(Received February 8, 2019, Revised November 29, 2019, Accepted December 12, 2019)

Abstract. Based on the dynamic tests of recycled aggregate concrete (RAC) short columns confined by the hoop reinforcement, the dynamic failure mechanism and the mechanical parameters related to the constitutive relation of confined recycled aggregate concrete (CRAC) were investigated thoroughly. The fracturing sections were relatively flat and smooth at higher strain rates rather than those at a quasi-static strain rate. With the increasing stirrup volume ratio, the crack mode is transitioned from splitting crack to slipping crack constrained with large transverse confinement. The compressive peak stress, peak strain, and ultimate strain increase with the increase of stirrup volume ratio, as well as the increasing strain rate. The dynamic confining increase factors of the compressive peak stress, peak strain, and ultimate strain increase by about 33%, 39%, and 103% when the volume ratio of hoop reinforcement is increased from 0 to 2%, but decrease by about 3.7%, 4.2%, and 9.1% when the stirrup spacing is increased from 20mm to 60mm, respectively. This sentence is rephrased as follows: When the stirrup volume ratios are up to 0.675%, and 2%, the contributions of the hoop confinement effect to the dynamic confining increase factors of the compressive peak strain and the compressive peak stress are greater than those of the strain rate effect, respectively. The dynamic confining increase factor (DCIF) models of the compressive peak stress, peak strain, and ultimate strain of CRAC are proposed in the paper. Through the confinement of the hoop reinforcement, the ductility of RAC, which is generally slightly lower than that of NAC, is significantly improved.

Keywords: recycled aggregate concrete (RAC) short column; confined recycled aggregate concrete (CRAC); dynamic confining effect; dynamic confining increase factor (DCIF); compressive peak stress; compressive peak strain; compressive ultimate strain

1. Introduction

Recycled aggregate concrete (RAC) technology has been investigated and popularized significantly in recent years. The basic properties of recycled coarse aggregate (RCA) (Li *et al.* 2004; Shatarat *et al.* 2018), and the static mechanical behaviors of RAC (Frondestou 1977; Sagoe-Crentsil and Brown 2001; ACI Committee 555 2002; Goksu *et al.* 2019;) have been studied systematically and analyzed theoretically. The brittleness of RAC is slightly higher than that of natural aggregate concrete (NAC), and it increases with the increase of RCA replacement ratio (R) (Xiao *et al.* 2005; Xiao 2008; Wang and Xiao 2017). Compared with NAC members, under the same conditions, the cracking load of RAC members with the inclined section is smaller than that of NAC members, and with the increase of R, the cracking load tends to decrease. The average width of the inclined crack of RAC members is slightly larger than that

of NAC members. The ultimate shear capacity of RAC members decreases with the increase of R (Xiao *et al.* 2012).

In terms of the characteristics of the loads and deformation of RAC, and considering the construction cost, adopting the confinement of the transverse hoop reinforcement in the design of RAC structure can greatly reduce the effects of brittleness and improve the shear behavior, ductility, plastic deformation, and energy dissipation capacity of RAC.

At present, a series of researches on the mechanical properties of confined recycled aggregate concrete (CRAC) under static loading conditions have been carried out worldwide. The static compression tests of RCA specimens confined by the steel tube and glass fiber reinforced plastics (GFRP) tube were conducted (Xiao *et al.* 2012; Huang *et al.* 2012). The investigation results indicate that the confining effect has an important effect on the mechanical properties of RAC, especially on its ductility, and the static constitutive relation model of CRAC was preliminarily determined. The static tests of recycled aggregate concrete-filled steel tubular (RACFST) beam/ column members under axial compression were carried out (Yang and Ma 2013; Chen *et al.* 2014). The results show that the

*Corresponding author, Ph.D., Professor
E-mail: changqingwang@tongji.edu.cn

^a Ph.D., Professor
E-mail: jzx@tongji.edu.cn

mechanical properties of RAC columns and beams are greatly improved by external steel tube restraint. A series of axial compression tests on carbon FRP (CFRP)-confined RAC/NAC cylinders were performed (Zhao *et al.* 2015; Chen *et al.* 2018). The test results indicate FRP (CFRP) confinement effectiveness is marginally affected by the use of recycled aggregate, and the compressive behavior of the two types of concrete can be almost equally well predicted by using stress-strain models originally proposed for FRP (CFRP)-confined NAC. The structural behavior of recycled aggregate concrete confined by spiral reinforcement subjected to static load excitations was investigated by Kim *et al.* (2018). It is indicated that the structural performance of recycled aggregate concrete specimens confined by steel spirals was similar to that of natural aggregate concrete specimens, regardless of the replacement ratio of recycled aggregates, the steel ratio and the yield strength of the spirals.

However, knowledge about the material properties and the structural behaviors of recycled aggregate concrete confined with hoop reinforcement subjected to dynamic loadings is insufficient. Few investigations on the stress-strain relation of CRAC under dynamic loading are performed in the existing literature. In fact, applications of RAC in civil and building engineering are rarely seen due to the immaturity of RAC technology.

In this study, based on the dynamic mechanical experimental tests of CRAC short columns with a square cross section confined by transverse hoops, the uniaxial compressive stress-strain complete curves of CRAC under dynamic monotonic loading conditions were obtained. The dynamic failure mechanism of CRAC under high strain rate was thoroughly analyzed. The influences for both the confinement of the transverse hoop reinforcement and the sensitivity of the strain rate on the cracks, the strength, and the deformation of CRAC were investigated deeply. Furthermore, the models of dynamic confining increase factor (DCIF) for the mechanical parameters (the compressive peak stress, the compressive peak strain, and the compressive ultimate strain of CRAC are initially proposed.

2. Test design

2.1 Material properties

Before conducting the mix proportion, the material properties for both natural coarse aggregate (NCA) and recycled coarse aggregate (RCA) were measured, as listed in Table 1. It is demonstrated that the water absorption of RCA is much higher than that of NCA. The fine aggregate used was river sand with a nominal particle diameter of 0.075–4.75 mm, which is classified as medium sand with the value of the fineness module of 2.4.

The sand before used was filtered by a sieve to remove impurities. The moisture content from the sand was removed by air drying. The coarse aggregate was sieved with the nominal size ranging from 4.75 mm to 10 mm, as shown in Fig. 1. The particle size distribution curve for RCA is illustrated in Fig. 2. It is implied that the particle

Table 1 Measured material properties of coarse aggregate

	Dust Type content (%)	Clay lump content (%)	Water absorption (%)	Moisture content (%)	Bulk density (kg/m ³)	Tight density (kg/m ³)	Apparent density (kg/m ³)
RCA	0.71	11.5	5.40	1.60	1200	1290	2600
NCA	0.80	7.6	1.80	0.40	1415	1525	2680



(a) Natural coarse aggregate



(b) Recycled coarse aggregate

Fig. 1 Coarse aggregate

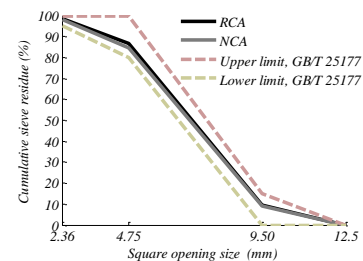


Fig. 2 Particle size distribution for both RAC and NAC

size distribution curves for both RCA and NCA are similar to each other. Moreover, both particle size distribution curves are kept within reasonable bounds according to China standard GB/T 25177 (2010). The measured yield strength of the steel reinforcement is 387.81 MPa.

2.2 Mix proportion

The strength grade of RAC is C30. Due to the high water absorption rate of RCA, it is necessary to increase the amount of water to assure the same effective water-cement ratio. This part of the water is called additional water, which was calculated through the measured effective water absorption (the water absorption from the natural state to the saturated surface dry) of the aggregates from Table 1. The water absorption and moisture content of RCA are 5.4% and 1.6% respectively (from Table 1). Ordinary Portland cement with a 28 days nominal compressive strength grade of 42.5 MPa was used. The water used was fresh tap water. The additive used was VIVID-500 (A)

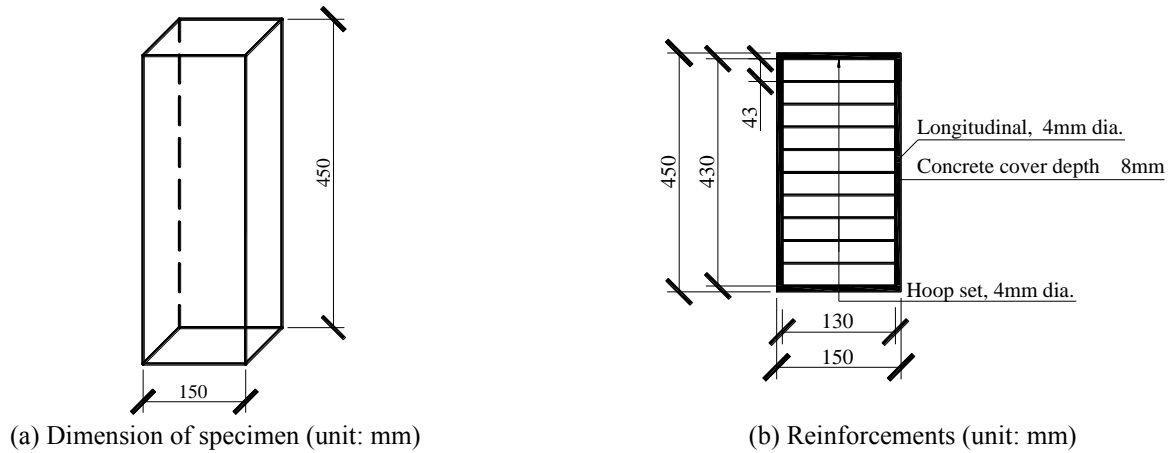


Fig. 3 the test units

Table 2 Mix proportion of RAC

Net water cement ratio	Sand ratio (%)	RCA (kg/m ³)	NCA (kg/m ³)	Sand (kg/m ³)	Cement (kg/m ³)	Net water content (kg/m ³)	Additional water (kg/m ³)
0.45	41%	852.1	0.0	592.1	485.5	218.5	32.4

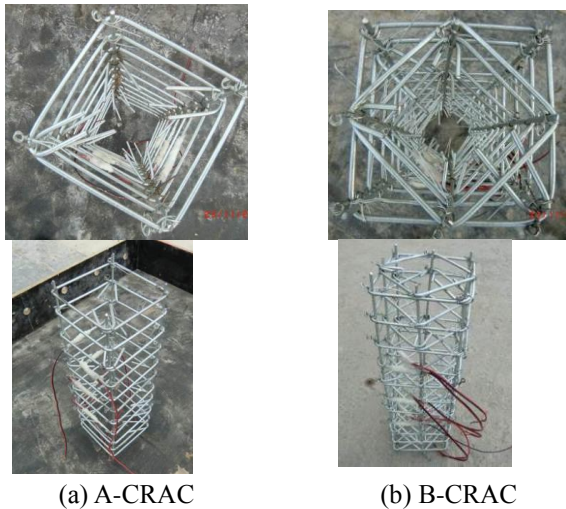


Fig. 4 Reinforcement cage fabricating

polycarboxylic superplasticizer and solid content is 40%. The collapsed slump of RAC was controlled between 180 mm and 200 mm. The mix proportions of RAC with RCA replacement ratios of 100% (i.e., all natural coarse aggregates are replaced by recycled coarse aggregates) were designed, and the contents of the various components of RAC per cubic meter were listed in Table 2.

2.3 Specimens

The test specimens were designed as short columns with a square cross-section of RAC that was 150 mm square and 450 mm high. The slenderness ratio of 3 to 1 was selected to avoid the influence of potential buckling and obtain a uniform stress distribution in the central region of the specimen. The specimens consisted of confined recycled aggregate concrete (CRAC) members and unconfined recycled aggregate concrete (URAC) members. There were two different types of stirrups A and B in CRAC specimens.



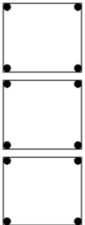
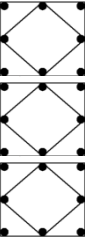
Fig. 5 Construction of RAC specimens

A-CRAC stands for the typical arrangement of square stirrups for 4-bar specimens, and B-CRAC stands for the typical arrangement of overlapping rhombic stirrups for 8-bar specimens. The dimension and reinforcements of the test units are shown in Fig. 3. All the specimens were manufactured in the laboratory. RAC was poured with formwork in wood in four batches and had been cured for 28 days under the room temperature condition. In addition, three groups of the prism (100mm×100mm×300mm) and three groups of the cube (150mm×150mm×150mm) were reserved for testing the material properties of RAC. Fig. 4 shows photos of the reinforcement cage fabricating. The typical construction photos are displayed in Fig.5. The specimen details are listed in Table 3.

2.4 Test setup and loading procedure

All experimental tests were conducted in an MTS 815.04 concrete testing system, which is an electro-hydraulic servo-controlled testing machine with a set of data acquisition systems. The uniaxial deformation of the test unit between the top and the bottom bearing plates was measured via the internal linear variable differential transformer (LVDT). In addition, external axial strain

Table 3 Design parameters of RAC specimens

Group	Strain rate (1/s) (Velocity mm/s)	Confined type	Volume stirrup ratio (%)	Sampling frequency (Hz)	Number
URAC-1	10^{-2} (4.5)	Unconfined	0	512	3
URAC-2	10^{-3} (0.45)	Unconfined	0	256	3
URAC-3	10^{-5} (0.0045)	Unconfined	0	12.8	3
A-CRAC-1	10^{-2} (4.5)		0.675	512	3
A-CRAC-2	10^{-3} (0.45)		0.675	256	3
A-CRAC-3	10^{-5} (0.0045)		0.675	12.8	3
B-CRAC-1	10^{-2} (4.5)		1.013	512	3
B-CRAC-2	10^{-3} (0.45)		1.013	256	3
B-CRAC-3	10^{-5} (0.0045)		1.013	12.8	3

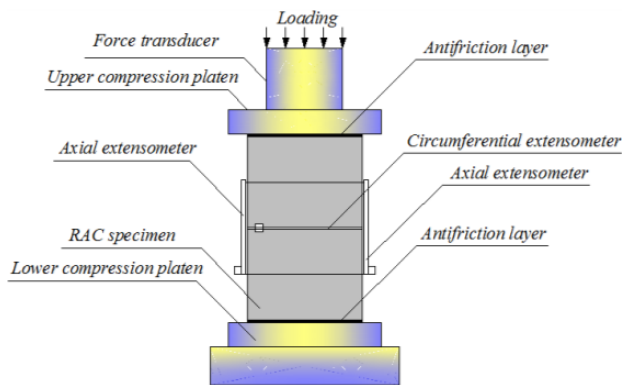


Fig. 6 The loading setup

measurement kits with a working range of ± 4.00 mm and a gauge length of 100 mm were installed to record the local longitudinal strain of RAC in the middle. The loading setup is shown in Fig. 6. After the preparation of the specimens and the testing machine, the tests were carried out at a series of typical controlled rates of longitudinal compressive strain of $10^{-5}/s$, $10^{-3}/s$, $10^{-2}/s$, and $10^{-1}/s$, which correspond to the loading rates of 0.0045mm/s, 0.45mm/s, 4.5mm/s, and 45mm/s, respectively. The low rate of strain, $10^{-5}/s$, is representative of the strain rate used in the quasi-static test condition, at which a group of RAC test units was tested, and compared to those with dynamic loading conditions. A medium rate of strain, $10^{-3}/s$, and higher rates of strain, $10^{-2}/s$ and $10^{-1}/s$, were employed to determine the sensitivity of the mechanical parameters of RAC, and can be also regarded as being indicative of the strain rate expected during the response of reinforced concrete subjected to strong earthquake motions (see also Bischoff and Perry 1991). The loading rate was kept constantly and monotonically during the test until the specimen failed in compression.

The strain of the hoop reinforcement was measured by the electric resistance strain gauge. Five hoops in the middle

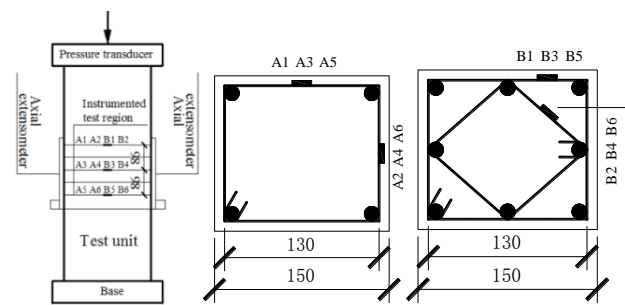


Fig. 7 Arrangement of measured hoop strain gauges

region of the specimen were selected, and the measuring points were arranged on every other stirrup. There were altogether six strain gauges were arranged in each specimen. The strain gauges were arranged from top to bottom and numbered successively as shown in Fig. 7. In addition, the experimental data from hoop reinforcement were acquired through the DH5922 dynamic signal test and analysis system. When a single computer control system is controlled, the experimental data from both DH5922 and MTS 815.04 test setup can be acquired synchronously.

3. Dynamic test

3.1 Failure pattern

Under the lower strain rate, the fractures mainly ran along with the interface between the coarse aggregates and the cement paste. However, few recycled coarse aggregates were penetrated by the cracks, as shown in Fig. 8 (a). Under a higher strain rate, a large number of recycled coarse aggregates were penetrated by some cracks. The fracturing sections were relatively flat and smooth at higher strain rates rather than those at the quasi-static strain rate, as shown in Fig. 8 (b) and Fig. 8 (c).

(a) Strain rate: $10^{-5}/s$ (b) Strain rate: $10^{-3}/s$ (c) Strain rate: $10^{-2}/s$

Fig. 8 Fracturing section



(a) URAC



(b) A-CRAC

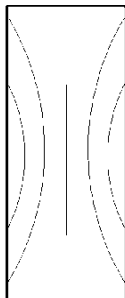


(c) B-CRAC

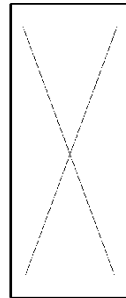


(d) Hoop reinforcement

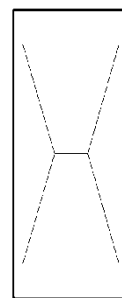
Fig. 9 Failure photos of the test specimens



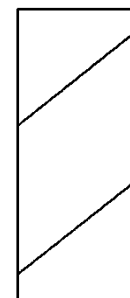
(a) Vertical cracks



(b) X-shaped cracks



(c) H-shaped cracks



(d) Slipping cracks

Fig. 10 Typical failure pattern

Fig. 9 shows the failure photos of the test specimens. The failure process of CRAC subjected to the dynamic loads went through five stages including elastic stage, elastic-plastic stage, yield stage, cracking penetration stage, and the stage of cover concrete spalling. The URAC specimens suffered serious damage and one or more main control cracks occurred when the axial strain reached 12×10^{-3} . However, the CRAC specimens suffered serious damage only when the axial strain reached 24×10^{-3} , but the specimens were able to still be kept as a whole due to the interconnection of the stirrups, longitudinal bars, and concrete. At the elastic stage, and the confinement effect of the stirrups was not reflected obviously. With the increasing load, approximately up to 40 percent of the peak load, the specimen suffered some damage, and the vertical or oblique cracks appeared at the ends of the specimen. Approximating the peak load, the existing cracks extended further and new cracks appeared, accompanied by the splitting sound of concrete. After the peak load, the spalling of the cover concrete occurred and the several main cracks formed, and the transverse strain of the core concrete increased significantly and the tensile damage occurred on the stirrups. The core concrete between the adjacent stirrups was crushed gradually, but due to the confinement of the stirrups, the bearing capacity of RAC in the core region

decreased slowly. When the axial strain reached about 24×10^{-3} , the stirrups bent horizontally exposed in the air induced by the squeezing effect of the core concrete as shown in Fig. 9 (d).

The failure patterns of RAC are different with the change of volume stirrup ratio. According to the failure mechanism of concrete (Ye and Ye 1995; Li *et al.* 2000), concrete cracks were usually divided into splitting crack and slipping crack. For URAC, the cracking mode belonged to the former. With the increasing volume ratio of the hoop reinforcement, the crack mode was transited from splitting crack to slipping crack constrained with large transverse confinement. According to the crack developing, the RAC specimens can be divided into the following failure patterns: (1) the vertical cracks, which are mainly parallel to the direction of the axial force, (Fig. 10 (a)); (2) the diagonal cracks connected to the horizontal cracks in the middle of the specimen each other to form X-shaped or H-shaped cracks. (Figs 10 (b) and 10 (c)); (3) oblique cracking slipping cracks (Fig. 10 (d)).

3.2 Experimental curves

The strength and deformation characteristics of the experimental stress-strain curves plotted in Fig. 11 are analyzed and compared.

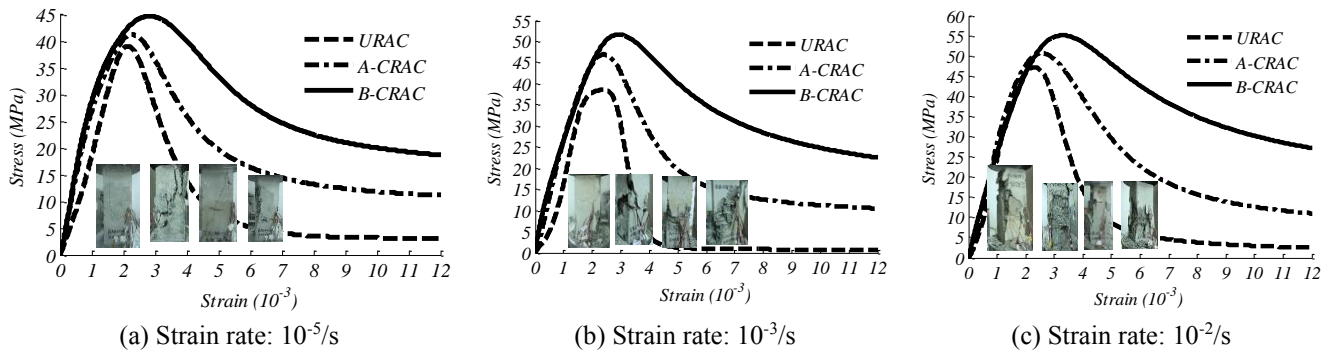


Fig. 11 Typical experimental curves of the stress-strain relation

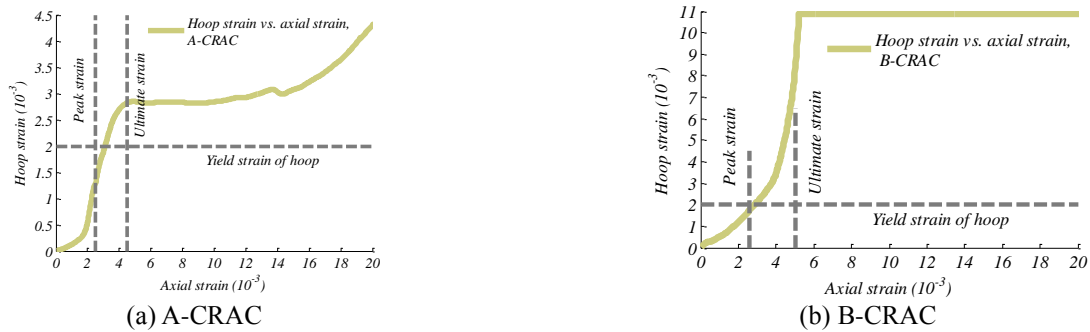


Fig. 12 Measured hoop strain vs. axial strain curves

Under the dynamic loading conditions, the shape and distribution of the uniaxial compressive stress-strain curves are in accord with those from quasi-static tests (Jin *et al.* 2005; Zeng *et al.* 2013), i.e., the experimental curves exhibit well-defined peak loads, as well as smooth and continuous descending branches after peak load.

Changing trend due to the RCA influence is similar to that in the quasi-static loading tests from the previous conclusions (Du *et al.* 2010). The test results show that, with the increase of R , the descending branch of stress-strain curve changes in a steeper trend indicating the brittleness of RAC increases obviously.

With the increasing strain rate, the compressive peak stress, the compressive peak strain, the initial compressive elastic modulus, the compressive ultimate strain (corresponding to the strain of 85% the compressive stress at the post-peak branch of the stress-strain curve), the stiffness of the descending branch (i.e., the slope along the path from the point of the compressive peak stress to the point of 85% the compressive peak stress at the post-peak branch of the stress-strain curve) and the energy absorption capacity (defined as the energy necessary to deform a given specimen to a specific strain, i.e., the area under the stress-strain curve) increase progressively. On the other hand, the deformability and ductility of RAC decrease with an increase in the strain rate. The strength enhancement found in this study as a result of the strain rate effect is consistent with those conclusions by Lu *et al.* (2014) and Xiao *et al.* (2015).

Substantial enhancement of peak compressive stress and critical strain of RAC are obtained as a result of the confinement of the hoop reinforcement. However, the initial

compressive elastic modulus and the stiffness of the descending branch decrease with an increase of volume stirrup ratio. The consistent strength enhancement found in these tests as a result of the confinement effect is in accord with those conclusions (Scott *et al.* 1982; Wee *et al.* 1996).

The more detailed information about the influence of the RCA replacement ratio, the strain rate, and the hoop reinforcement confinement on the characteristic parameters of the stress-strain curve was analyzed and described in the following sections.

The measured curves of hoop strain vs. axial strain are illustrated in Fig. 12. In the figure, the horizontal axis stands for the measured longitudinal compressive strain, and the vertical axis denotes the measured hoop strain. The horizontal dashed line indicates the tensile yield strain of the hoop reinforcement. The vertical dashed lines stand for the longitudinal compressive peak strain and ultimate strain, respectively. It is observed that the strain is still lower than the yield strain of the hoop reinforcement when the longitudinal strain is up to the compressive peak strain of CRAC. The hoop bars just step into the hardening stage when the longitudinal strain is close to the compressive ultimate strain. It is indicated that, through the confinement of the hoop reinforcement, the ductility of RAC, which is generally slightly lower than that of NAC, is significantly improved.

4. Dynamic confinement effect

In order to analyze and quantify the effects of the strain rate and the hoop reinforcement confinement on the

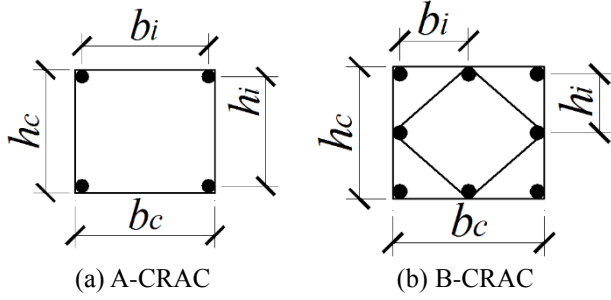


Fig. 13 Model parameters related to the steel bars

mechanical properties of RAC, the dynamic confining increase factor (DCIF) is introduced in this paper, that is, the ratio of the mechanical index of CRAC under the dynamic loading to that of URAC under the quasi-static loading.

4.1 Compressive Peak stress

The compressive peak stress is an important mechanical parameter to describe the mechanical properties of concrete, which is the mean value of the peak stresses in each group of specimens as shown in Fig. 11. It can be seen that the dynamic confining effect on the compressive peak stress is very prominent. In order to quantify the influence of the dynamic confining effect, through the regression analysis of the data from the dynamic tests, the empirical formula of DCIF of the compressive peak stress is proposed in the present paper. The proposed calculation function model derived from experimental data is described and expressed in equation (1). The influences for both the strain rate and the hoop reinforcement confinement are couple into the proposed model. The proposed function model curves by the author against experimental results are illustrated in Fig. 14.

$$c_{f_{dc}} = \left(\frac{\dot{\varepsilon}_c}{\dot{\varepsilon}_{c0}} \right)^{\alpha_a \left(\frac{1}{\beta_a + 30\theta_a} \right)} \cdot \left[1 + \psi \left(1 - \frac{s}{2b_c} \right) \left(1 - \frac{s}{2h_c} \right) \left(1 - \frac{b_i}{3b_c} - \frac{h_i}{3h_c} \right) \frac{\rho_{sv} f_{y0}}{f_{c0}} \right] \quad (1)$$

where $c_{f_{dc}}$ stands for the dynamic constraint factor of the compressive peak stress; α_a , β_a , θ_a , and ψ are model constants, are attained from the dynamic test and listed in Table 4; f_{c0} and f_{y0} donate the compressive peak stress of URAC and the yield strength of the hoop reinforcement under the quasi-static loading condition (in MPa), respectively; ρ_{sv} is the stirrup volume ratio (%); s represents the stirrup spacing (mm); b_c and h_c represent the center to center spacing of the stirrups in two horizontal directions in the cross-section (see Fig. 13 (a)), in mm, respectively; b_i and h_i represent the center to center spacing of the longitudinal bars in two horizontal directions in the cross-section (see Fig. 13 (b)), in mm, respectively; $\dot{\varepsilon}_c$ represents the strain rate applied to RAC; $\dot{\varepsilon}_{c0}$ stands for the quasi-static strain rate is equal to $1 \times 10^{-5}/s$ in this study.

Table 4 DCIF model parameters of the compressive peak stress

Parameters				Model function
α_a	β_a	θ_a	ψ	$c_{f_{dc}}$
6.664	6.943	8.656	3.2604	

Table 5 Peak stress comparison of prediction from the proposed model with experimental results

Specimens	Strain rates (1/s)	Model (MPa)	Test (MPa)	$\left \frac{\text{Model}-\text{Test}}{\text{Test}} \right $ (%)
URAC-1	10^{-2}	42.18	46.95	10.17
URAC-2	10^{-3}	39.82	40.48	1.64
URAC-3	10^{-5}	35.49	38.46	7.73
A-CRAC-1	10^{-2}	46.89	47.92	2.16
A-CRAC-2	10^{-3}	44.26	47.39	6.59
A-CRAC-3	10^{-5}	39.45	41.65	5.27
B-CRAC-1	10^{-2}	49.25	53.70	8.30
B-CRAC-2	10^{-3}	46.49	46.96	1.00
B-CRAC-3	10^{-5}	41.44	42.12	1.63

Based on the proposed formula in equation (1), a comparison of the compressive peak stress between the predicted value and the experiment result is listed in Table 5. The predicted errors under different strain rates are analyzed and illustrated in Fig. 15. The minimum predicted error is 1.0 % occurred in B-CRAC specimen at the strain rate of $10^{-3}/s$. The maximum predicted error is 10.1 % occurred in the URAC specimen at the strain rate of $10^{-2}/s$. The average predicted error for all specimens is 4.9 %. Good agreement implied that the proposed DCIF model of the compressive peak stress is reasonable and acceptable.

The confinement effect of the hoop reinforcement on the mechanical parameters is dependent on many factors. The early research results (Scott *et al.* 1982; Mander *et al.* 1988; Wee *et al.* 1996; Li *et al.* 2000) found that the volume ratio of transverse reinforcements, the type of hoop sets (i.e., the shape, spacing), the spacing of the longitudinal bars, the compressive strength of plain concrete, and the yielding strength of the transverse and longitudinal reinforcement have a significant influence on the behaviors of concrete.

Based on the verified predicted model, the influences of the volume ratio and the spacing of the hoop reinforcement on the compressive peak stress were analyzed emphatically, as shown in Fig. 16. It can be seen from the curves that DCIF increases with the increase of stirrup volume ratio (Fig. 16 (a)), but decreases with the increase of the stirrup spacing (Fig. 16 (b)). DCIF of the compressive peak stress increased by about 33% when the volume ratio of hoop reinforcement was increased from 0 to 2%, whereas the DCIF value decreased by about 3.7% when the stirrup spacing was increased from 20mm to 60mm as provided in Table 6. The contribution ratio defined as the ratio of the increased DCIF value induced by the stirrup confinement effect to that induced by the strain rate effect was listed in Table 6. It is found that the

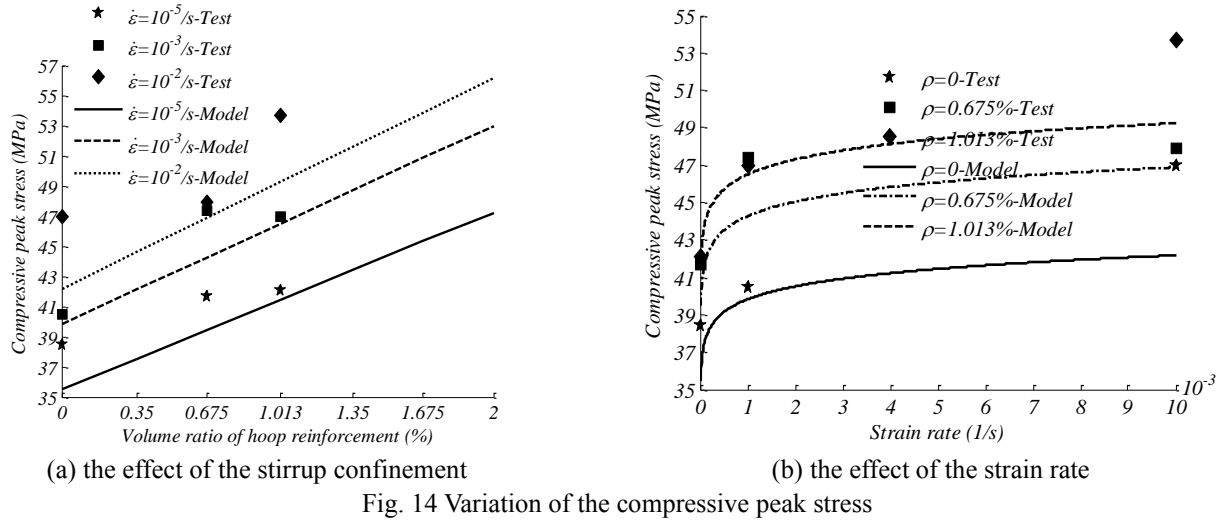


Fig. 14 Variation of the compressive peak stress

Table 6 DCIF and contribution ratio of the compressive peak stress under different given conditions

Strain rate (1/s)	$s=43\text{mm}, b_c=130\text{mm}, h_c=130\text{mm}, b_i=61\text{mm}, h_i=61\text{mm},$ $f_{c0}=35.49\text{MPa}, f_{y0}=387.81\text{MPa}$				$\rho_{sv}=0.675\%, b_c=130\text{mm}, h_c=130\text{mm}, b_i=61\text{mm}, h_i=61\text{mm},$ $f_{c0}=35.49\text{MPa}, f_{y0}=387.81\text{MPa}$			
	$\rho_{sv} (\%)$				$s (\text{mm})$			
	0	0.675	1.013	2	20	30	40	60
10^{-5}	1.000	1.115	1.173	1.341	1.141	1.129	1.118	1.098
10^{-2}	1.189	1.325	1.394	1.594	1.356	1.342	1.329	1.305
Contribution ratio	0.00/1.00	0.35/0.65	0.44/0.56	0.57/0.43	0.40/0.60	0.38/0.62	0.36/0.64	0.32/0.68

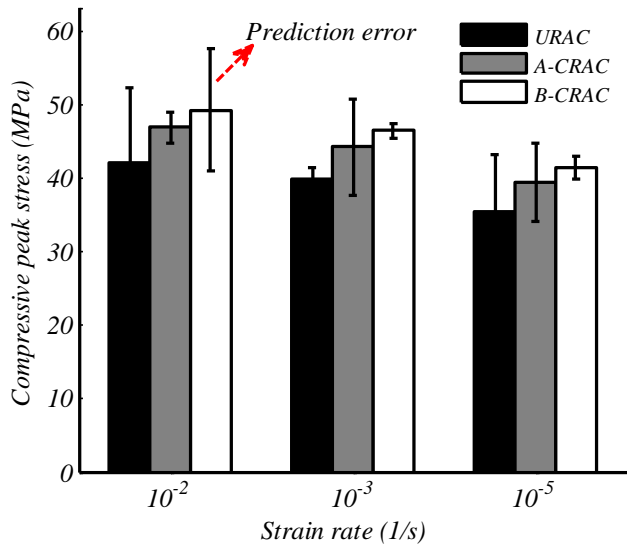


Fig. 15 The peak stress and the predicted error

contribution of hoop confinement to the compressive peak stress increases with the increase of the stirrup volume ratio but decreases with the increasing stirrup spacing. When the stirrup volume ratio is up to 2%, the contribution of the hoop confinement effect to DCIF of the compressive peak stress is greater than that of the strain rate effect.

4.2 Compressive peak strain

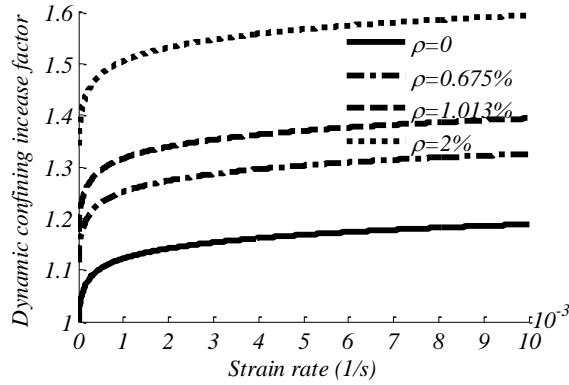
The compressive peak strain is the strain corresponding to the peak stress. The influence of the strain rate on the

compressive peak strain of NAC is un-noticeably in the previous findings (Scott *et al.* 1982; Zeng *et al.* 2013). In the paper, the effects for both the strain rate sensitivity and the hoop reinforcement confinement on the compressive peak strain of RAC were investigated thoroughly.

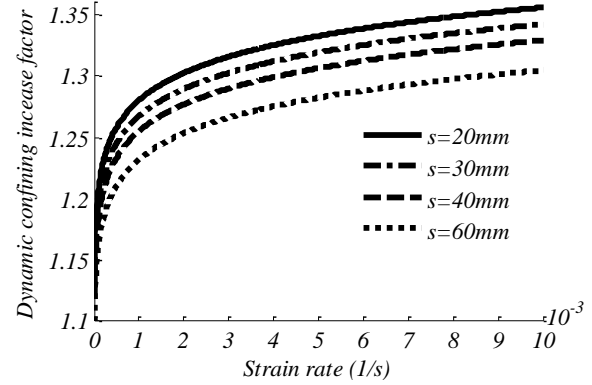
In order to quantify the influence of the dynamic confining effect of the compressive peak strain, through the regression analysis of the data from the dynamic tests, the empirical formula of DCIF of the compressive peak strain is developed and suggested in the present paper. The proposed prediction function model derived from experimental data is described and expressed in equation (2). The influences for both the strain rate and the hoop reinforcement confinement are also couple into the proposed model. The proposed function model curves by the author against experimental results are illustrated in Fig. 17.

$$c_{\varepsilon_{dc}} = \left(\frac{\dot{\varepsilon}_c}{\dot{\varepsilon}_{c0}} \right)^\phi \cdot \left[1 + \vartheta \left(1 - \frac{s}{2b_c} \right) \left(1 - \frac{s}{2h_c} \right) \left(1 - \frac{b_i}{3b_c} - \frac{h_i}{3h_c} \right) \frac{\rho_{sv} f_{y0}}{300} \right] \quad (2)$$

where $c_{\varepsilon_{dc}}$ represents the dynamic confining factor of the compressive peak strain; The model parameters, ϕ and ϑ , which can be determined experimentally and listed in Table 7. The definitions of other model parameters are the same as those in equation (1).

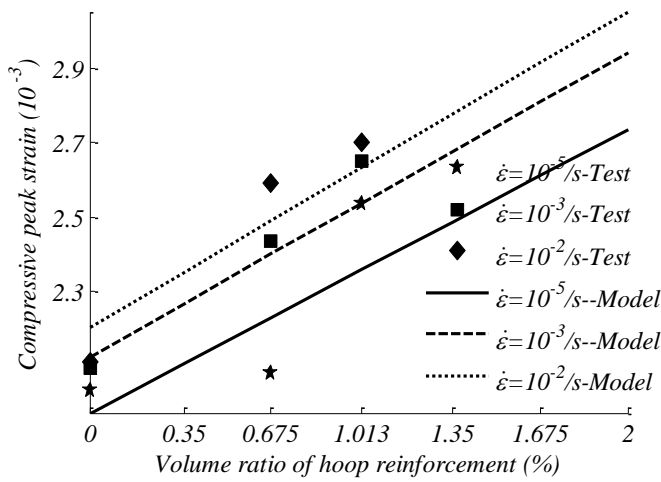


(a) the influence of the stirrup volume ratio

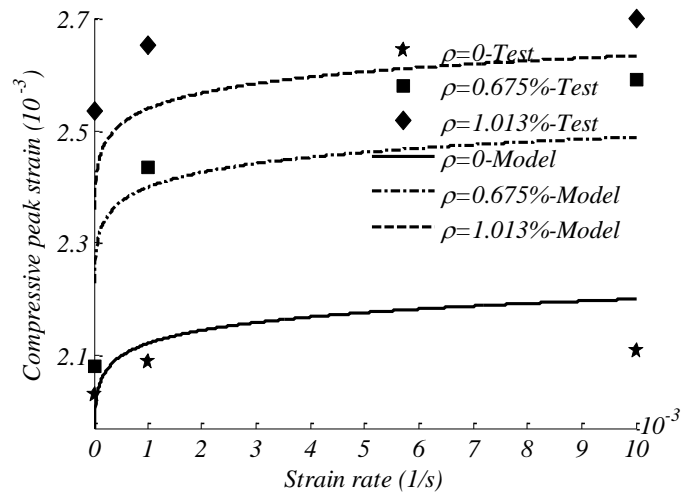


(b) the influence of the stirrup spacing

Fig. 16 DCIF curves of the compressive peak stress



(a) the effect of the stirrup confinement



(b) the effect of the strain rate

Fig. 17 Variation of the compressive peak strain

Table 7 DCIF model parameters of the compressive peak strain

Parameters		Model function
ϕ	ϑ	
0.01597	32.389	$c_{\varepsilon_{dc}}$

In order to support the suggested model of DCIF from equation (2), a comparison of the compressive peak strain between the predicted values and the experiment results for test specimens is performed and listed in Table 8. The predicted errors under the different strain rates are illustrated in Fig. 18.

It is observed that the minimum predicted error is 1.4 % occurred in A-CRAC specimen at the strain rate of $10^{-3}/s$. The maximum predicted error is 7.1 % occurred in A-CRAC specimen at the strain rate of $10^{-5}/s$. The average predicted error for all specimens is 3.8 %.

Thus, the good agreement indicates that the proposed empirical formula of DCIF is reasonable and applicable to describe the changing law of the compressive peak strain of recycled aggregate concrete subjected to the excitation of the dynamic loading.

Table 8 Peak strain comparison of prediction from the proposed model with experimental results

Specimens	Strain rates (1/s)	Model (10^{-3})	Test (10^{-3})	$\left \frac{\text{Model}-\text{Test}}{\text{Test}} \right $ (%)
URAC-1	10^{-2}	2.200	2.109	4.32
URAC-2	10^{-3}	2.121	2.090	1.47
URAC-3	10^{-5}	1.970	2.030	2.94
A-CRAC-1	10^{-2}	2.489	2.590	3.90
A-CRAC-2	10^{-3}	2.399	2.434	1.43
A-CRAC-3	10^{-5}	2.229	2.080	7.16
B-CRAC-1	10^{-2}	2.634	2.701	2.50
B-CRAC-2	10^{-3}	2.539	2.651	4.24
B-CRAC-3	10^{-5}	2.359	2.535	6.96

In the same way, based on the verified predicted model, the influences of the volume ratio and the spacing of the hoop reinforcement on the compressive peak strain were analyzed further, as shown in Fig. 19. It is demonstrated that DCIF increases with the increase of stirrup volume ratio (Fig. 19 (a)), but decreases with the increase of the stirrup spacing (Fig. 19 (b)). As presented in Table 9, DCIF

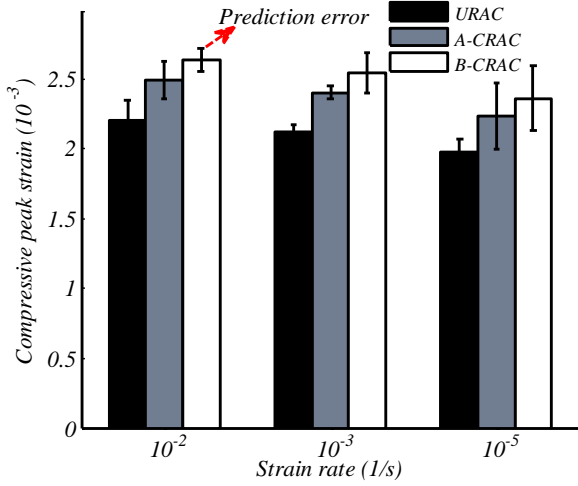


Fig. 18 The peak strain and the predicted error

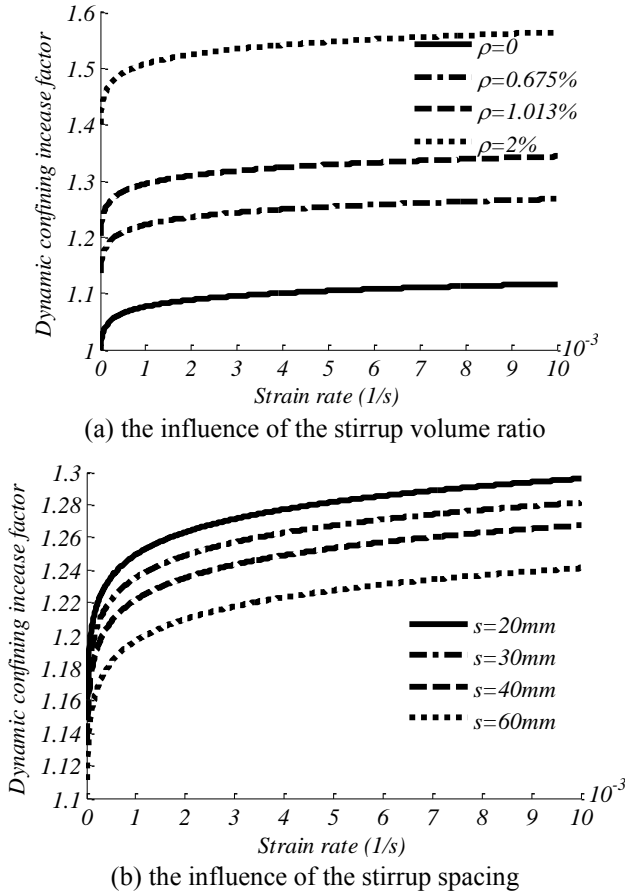


Fig. 19 DCIF curves of the compressive peak strain

of the compressive peak strain increases by about 39% when the volume ratio of hoop reinforcement is increased from 0 to 2% but decreases by about 4.2% when the stirrup spacing is increased from 20mm to 60mm. It is found that the contribution of hoop confinement to the compressive peak strain increases with the increase of the stirrup volume ratio or the decrease of the stirrup spacing. When the stirrup volume ratio is up to 0.675%, the contribution of the hoop confinement effect to DCIF of the compressive peak strain is greater than that of the strain rate effect.

Table 9 DCIF and contribution ratio of the compressive peak strain under different given conditions

Strain rate (1/s)	$s=43\text{ mm}, b_c=130\text{ mm},$ $h_c=130\text{ mm}, b_i=61\text{ mm}, h_i=61\text{ mm},$ $f_{ci}=35.49\text{ MPa}$ $f_{yi}=387.81\text{ MPa}$				$\rho_{sv}=0.675\%, b_c=130\text{ mm},$ $h_c=130\text{ mm}, b_i=61\text{ mm}, h_i=61\text{ mm},$ $f_{ci}=35.49\text{ MPa}$ $f_{yi}=387.81\text{ MPa}$			
	$\rho_{sv}\text{ (%)}$				$s\text{ (mm)}$			
	0	0.675	1.013	2	20	30	40	60
10^{-5}	1.000	1.135	1.203	1.401	1.161	1.147	1.135	1.112
10^{-2}	1.117	1.268	1.343	1.564	1.296	1.281	1.267	1.241
Contribution ratio	0.00/1.00	0.51/0.49	0.59/0.41	0.71/0.29	0.54/0.46	0.52/0.48	0.50/0.50	0.46/0.54

Table 10 DCIF model parameters of the ultimate strain

Parameters	Model function
φ	ϖ
0.002	85.5436
	$c_{\varepsilon_{2dc}}$

4.3 Compressive ultimate strain

The reports about the effect of dynamic confinement on the compressive ultimate strain of concrete have been very poor. Based on the dynamic tests, the effects of both the hoop reinforcement confinement and the strain rate sensitivity on the compressive ultimate strain of RAC were analyzed intensively in the present paper.

In the same way, in order to quantify the influence of the dynamic confining effect of the compressive ultimate strain, through the regression analysis of the data from the dynamic tests, the empirical formula of DCIF of the compressive ultimate strain is developed and suggested. The proposed prediction function model derived from experimental data is described and expressed in equation (3). The influences for both the strain rate and the hoop reinforcement confinement are also couple into the proposed model. The proposed function model curves by the author against experimental results are illustrated in Fig. 20.

$$c_{\varepsilon_{2dc}} = \left(\frac{\dot{\varepsilon}_c}{\dot{\varepsilon}_{c0}} \right)^{\varphi} \cdot \left[1 + \varpi \left(1 - \frac{s}{2b_c} \right) \left(1 - \frac{s}{2h_c} \right) \left(1 - \frac{b_i}{3b_c} - \frac{h_i}{3h_c} \right) \frac{\rho_{sv} f_{y0}}{300} \right] \quad (3)$$

where $c_{\varepsilon_{2dc}}$ represents the dynamic confining factor of the compressive ultimate strain; The model parameters, φ and ϖ , which can be determined experimentally and listed in Table 10. The definitions of other model parameters are the same as those in equations (1) and (2).

In order to validate the suggested function model of DCIF from equation (3), a comparison of the compressive ultimate strain between the predicted values and the experiment results is carried out and listed in Table 11. The predicted errors under the different strain rates are illustrated in Fig. 21.

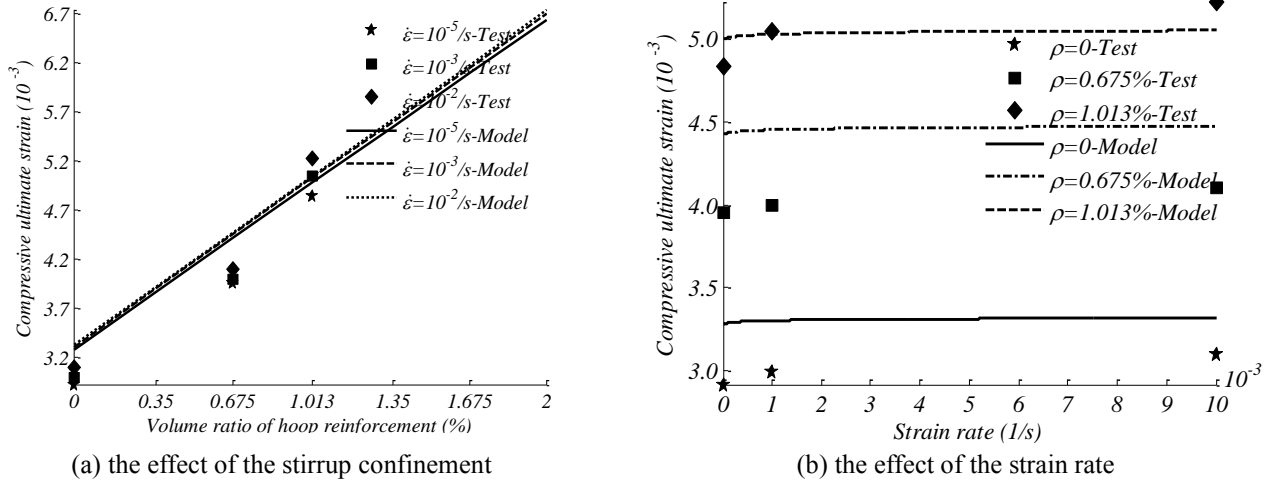


Fig. 20 Variation of the compressive ultimate strain

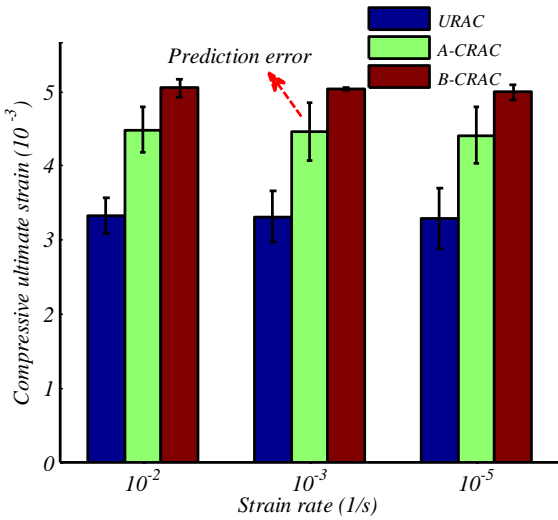


Fig. 21 The peak strain and the predicted error

Table 11 Ultimate strain comparison of prediction from the proposed model with experimental results

Specimens	Strain rates (1/s)	Model (10 ⁻³)	Test (10 ⁻³)	$\left \frac{\text{Model}-\text{Test}}{\text{Test}} \right $ (%)
URAC-1	10 ⁻²	3.323	3.099	7.20
URAC-2	10 ⁻³	3.308	2.995	10.42
URAC-3	10 ⁻⁵	3.278	2.920	12.26
A-CRAC-1	10 ⁻²	4.476	4.098	9.21
A-CRAC-2	10 ⁻³	4.455	3.995	11.51
A-CRAC-3	10 ⁻⁵	4.403	3.949	11.51
B-CRAC-1	10 ⁻²	5.040	5.221	3.47
B-CRAC-2	10 ⁻³	5.030	5.044	0.29
B-CRAC-3	10 ⁻⁵	4.984	4.832	3.15

It is observed that the minimum predicted error is 0.3 % occurred in B-CRAC specimen at the strain rate of 10⁻³/s. The maximum predicted error is 11.5 % occurred in A-CRAC specimen at the strain rate of 10⁻⁵/s. The average predicted error for all specimens is 7.6 %. It is implied that the predictions agree well with the experimental results.

Likewise, based on the verified predicted model, the influences of both the volume ratio and the spacing of the hoop reinforcement on the compressive ultimate strain were also analyzed, as shown in Fig. 22. It is indicated that DCIF increases with the increasing stirrup volume ratio (Fig. 22 (a)), as well as the decrease of the stirrup spacing (Fig. 22 (b)). From Table 12, it can be seen that DCIF of the compressive ultimate strain increases by about 103% when the volume ratio of hoop reinforcement is increased from 0 to 2% but decreases by about 9.1% when the stirrup spacing is increased from 20mm to 60mm. It is found that the contribution of hoop confinement to the compressive ultimate strain increases with the increase of the stirrup volume ratio or the decrease of the stirrup spacing. The contribution of the hoop confinement effect to DCIF of the compressive ultimate strain is much greater than that of the strain rate effect.

Through analyzing and comparison of the contribution ratios presented in Tables 6, 9 and 12, it is implied that the influence of the strain rate sensitivity on the compressive peak stress is the most significant, followed by the compressive peak strain, and the compressive ultimate strain. On the other hand, the influence of the hoop reinforcement confinement on the compressive ultimate strain is the biggest, followed by the compressive peak strain, and the compressive peak stress.

5. Summary and conclusions

Based on the dynamic tests of recycled aggregate concrete short columns, the failure pattern and the mechanical parameters were investigated comprehensively. The main conclusions are summarized as follows.

- The compressive peak stress increases with the increase of volume ratio of the hoop reinforcement, as well as the increasing strain rate. A quantified dynamic confining increase factor model of the compressive peak stress of RAC is proposed and expressed in equation (1). The contribution of the hoop confinement effect to the compressive peak stress is greater than that of the strain rate effect when the stirrup volume ratio is up to 2%.

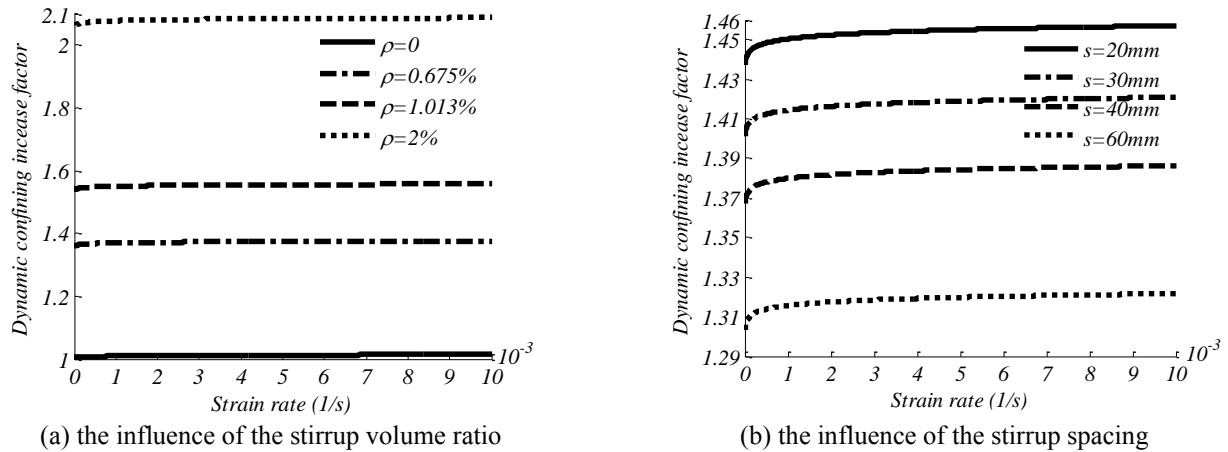


Fig. 22 DCIF curves of the compressive ultimate strain

Table 12 DCIF and contribution ratio of the compressive ultimate strain under different given conditions

Strain rate (1/s)	$s=43\text{mm}, b_c=130\text{mm}, h_c=130\text{mm}, b_f=61\text{mm}, h_f=61\text{mm},$ $f_{c0}=35.49\text{MPa}, f_{y0}=387.81\text{MPa}$				$\rho_{sv}=0.675\%, b_c=130\text{mm}, h_c=130\text{mm}, b_f=61\text{mm}, h_f=61\text{mm},$ $f_{c0}=35.49\text{MPa}, f_{y0}=387.81\text{MPa}$			
	ρ_{sv} (%)				s (mm)			
	0	0.675	1.013	2	20	30	40	60
10^{-5}	1.000	1.357	1.536	2.059	1.437	1.401	1.367	1.304
10^{-2}	1.014	1.376	1.558	2.087	1.457	1.421	1.386	1.322
Contribution ratio	0.00/1.00	0.95/0.05	0.96/0.04	0.97/0.03	0.96/0.04	0.95/0.04	0.95/0.04	0.94/0.06

- A quantified dynamic confining increase factor model of the compressive peak strain of RAC is suggested and expressed in equation (2). When the stirrup volume ratio is up to 0.675%, the contribution of the hoop confinement effect to the compressive peak strain is greater than that of the strain rate effect.

- A quantified dynamic confining increase factor model of the compressive ultimate strain of RAC is put forward and expressed in equation (3). The influence of the strain rate sensitivity on the compressive peak stress is the most significant, followed by the compressive peak strain, and the compressive ultimate strain. On the other hand, the influence of the hoop reinforcement confinement on the compressive ultimate strain is the biggest, followed by the compressive peak strain, and the compressive peak stress.

Acknowledgments

The authors wish to acknowledge the financial support from Project funded by the Fundamental Research Funds for the Central Universities (2018XKQYMS24).

References

- ACI Committee 555 (2002), "Removal and Reuse of Hardened Concrete", *ACI Mater. J.*, **99**(3), 300-325.
- Bischoff, P.H. and Perry, S.H. (1991), "Compressive behavior of concrete at high strain rates", *Mater. Struct.*, **24**(6), 425-450. <https://doi.org/10.1007/BF02472016>.
- Chen, G.M., Zhang, J.J., Jiang, T., Lin, C.J. and He, Y.H. (2018), "Compressive behavior of CFRP-confined recycled aggregate concrete in different-sized circular sections", *J. Compos. Construct.*, **22**(4), 1-12.

- [https://doi.org/10.1061/\(ASCE\)CC.1943-5614.0000859](https://doi.org/10.1061/(ASCE)CC.1943-5614.0000859).
- Chen, Z.P., Xu, J.J., Xue, J.Y. and Su, Y.S. (2014), "Performance and calculations of recycled aggregate concrete-filled steel tubular (RACFST) short columns under axial compression", *J. Steel Struct.*, **14**(1), 31-42. <https://doi.org/10.1007/s13296-014-1005-5>.
- Du, T., Wang, W.H., Liu, Z.X., Lin, H.L. and Guo, T.P. (2010), "The Complete Stress-strain Curve of Recycled Aggregate Concrete under Uniaxial Compression Loading", *Journal of Wuhan University of Technology-Materials Science Edition*, **25**(5), 862-865. <https://doi.org/10.1007/s11595-010-0109-9>.
- Frondestou, Y. (1977), "Waste concrete as aggregate concrete for new concrete", *J. ACI*, 212-219.
- GB/T 25177 (2010), Recycled Coarse Aggregate for Concrete, Ministry of Housing and Urban-Rural Development of the People's Republic of China; Beijing, China.
- Goksu, C., Saribas, I., Binbir, E., Akkaya, Y. and Ilki, A. (2019), "Structural performance of recycled aggregates concrete sourced from low strength concrete", *Struct. Eng. Mech.*, **69**(1), 77-93. <https://doi.org/10.12989/sem.2019.69.1.077>.
- Huang, Y. J., Xiao, J. Z. and Zhang, C. (2012), "Theoretical study on mechanical behavior of steel confined recycled aggregate concrete", *J. Construct. Steel Res.*, **76**, 100-111. <https://doi.org/10.1016/j.jcsr.2012.03.020>.
- Jin, X., Shen, Y. and Li, Z. (2005), "Behaviour of high- and normal-strength concrete at early ages", *Mag. Concrete Res.*, **57**(6), 339-345. <https://doi.org/10.1680/macr.2005.57.6.339>.
- Kim, S.W., Lee, B.S., Kim, Y.S., Lee, S.H. and Kim, K.H. (2018), "Structural performance of recycled aggregate concrete confined by spiral reinforcement", *J. Asian Architecture Building Eng.*, **17**(3), 541-548. <https://doi.org/10.3130/jaabe.17.541>.
- Li, B., Park, R. and Tanaka, H. (2000), "Constitutive behavior of high-strength concrete under dynamic loads", *ACI Struct. J.*, **97**(4), 619-629.
- Li, J. B., Xiao, J.Z. and Sun, Z.P. (2004), "Properties of recycled coarse aggregate and its influence on recycled concrete", *J.*

- Building Mater.*, **7**(4), 390-395.
- Lu, Y. B., Chen, X., Teng, X. and Zhang, S. (2014), "Dynamic compressive behavior of recycled aggregate concrete based on split Hopkinson pressure bar tests", *Latin American J. Solids Struct.*, **11**(1), 131-141. <https://doi.org/10.1590/S1679-78252014000100008>.
- Mander, J.B., Priestley, M.J.N. and Park, R. (1988), "Theoretical stress-strain model for confined concrete", *J. Struct. Eng. ASCE*, **114**(8), 1804-1826. [https://doi.org/10.1061/\(ASCE\)0733-9445\(1988\)114:8\(1804\)](https://doi.org/10.1061/(ASCE)0733-9445(1988)114:8(1804)).
- Sagoe-Crentsil, K.K. and Brown, T.T. (2001), "Performance of concrete made with commercially produced coarse recycled concrete aggregate", *Cement Concrete Res.*, **31**, 707-712. [https://doi.org/10.1016/S0008-8846\(00\)00476-2](https://doi.org/10.1016/S0008-8846(00)00476-2).
- Scott, B.D., Park, R. and Priestley, M.J.N. (1982), "Stress-strain behavior of concrete confined by overlapping hoops at low and high strain rates", *ACI J.*, **79**(2), 13-27.
- Shatarat, N. K., Katkhuda, H. N., Hyari, K. H. and Asi, I. (2018), "Effect of using recycled coarse aggregate and recycled asphalt pavement on the properties of pervious concrete", *Struct. Eng. Mech.*, **67**(3), 283-290. <https://doi.org/10.12989/sem.2018.67.3.283>.
- Wang, C.Q. and Xiao, J.Z. (2017), "Rate Dependence of Confined Recycled Aggregate Concrete", *ACI Struct. J.*, **114**(6), 1557-1567.
- Wee, T.H., Chin, M.S. and Mansur, M.A. (1996), "Stress-strain relationship of high-strength concrete in compression", *J. Mater. Civil Eng.*, **8**(2), 70-76. [https://doi.org/10.1061/\(ASCE\)0899-1561\(1996\)8:2\(70\)](https://doi.org/10.1061/(ASCE)0899-1561(1996)8:2(70)).
- Xiao, J. Z. (2008), *Recycled Concrete*, Chinese Building Press, Beijing, China.
- Xiao, J. Z., Huang, Y.J., Yang, J. and Zhang, C. (2012), "Mechanical properties of confined recycled aggregate concrete under axial compression", *Construct. Build. Mater.*, **26**(1), 591-603. <https://doi.org/10.1016/j.conbuildmat.2011.06.062>.
- Xiao, J. Z., Li, J. B. and Zhang, C. (2005), "Mechanical properties of recycled aggregate concrete under uniaxial loading", *Cement Concrete Res.*, **35**, 1187-1194. <https://doi.org/10.1016/j.cemconres.2004.09.020>.
- Xiao, J.Z., Li, L., Shen, L.M. and Poon, C.S. (2015), "Compressive behaviour of recycled aggregate concrete under impact loading", *Cement Concrete Res.*, **71**, 46-55. <https://doi.org/10.1016/j.cemconres.2015.01.014>.
- Xiao, J.Z., Xie, H. and Yang, Z.J. (2012), "Aggregate interlock and Shear transfer across a crack in recycled aggregate concrete", *Cement Concrete Res.*, **42**(5), 700-709. <https://doi.org/10.1016/j.cemconres.2012.02.006>.
- Yang, Y.F. and Ma, G.L. (2013), "Experimental behaviour of recycled aggregate concrete filled stainless steel tube stub columns and beams", *Thin-Wall. Struct.*, **66**, 62-75. <https://doi.org/10.1016/j.tws.2013.01.017>.
- Ye, Y.H. and Ye, L.P. (1995), "Failure mechanism of high-strength concrete confined by stirrups", *Jiangsu Construction*, **3**, 5-9.
- Zeng, S.J., Ren, X.D. and Li, J. (2013), "Triaxial Behavior of Concrete Subjected to Dynamic Compression", *J. Struct. Eng., ASCE*, **139**(9), 1582-1592. [https://doi.org/10.1061/\(ASCE\)ST.1943-541X.0000686](https://doi.org/10.1061/(ASCE)ST.1943-541X.0000686).
- Zhao, J.L., Yu, T. and Teng, J.G. (2015), "Stress-strain behavior of FRP-confined recycled aggregate concrete", *J. Compos. Construct.*, **19**(3), 1-11. [https://doi.org/10.1061/\(ASCE\)CC.1943-5614.0000513](https://doi.org/10.1061/(ASCE)CC.1943-5614.0000513).